Analysis of parameters distribution of EEG signals for five epileptic seizure phases modeled by duffing Van der Pol oscillator

Beata Szuflitowska[0000-0002-5825-7234] and Przemyslaw Orlowski[0000-0001-6407-9668]

West Pomeranian University of Technology in Szczecin, Sikorskiego 37, 70-313 Szczecin, Poland
bszuflitowska@zut.edu.pl

Abstract. Complex temporal epilepsy belongs to the most common type of brain disorder. Nevertheless, the wave patterns of this type of seizure, especially associated with behavioral changes, are difficult to interpret clinically. A helpful tool seems to be the statistical and time-frequency analysis of modeled epilepsy signals. The main goal of the study is the application of the Van der Pol model oscillator to study brain activity and intra-individual variability during complex temporal seizures registered in one patient. The achievement of the article is the confirmation that the statistical analysis of optimal values of three pairs of parameters of the duffing Van der Pol oscillator model enables the differentiation of the individual phases of the seizure in short-period seizure waves. In addition, the article attempts to compare the real signals recorded during the attack and modeled using frequency and time-frequency analysis. Similarities of power spectra and entropy samples of real and generated signals in low-frequency values are noted, and differences in higher values are explained about the clinical interpretation of the records.

Keywords: Van der Pol oscillator, EEG, parameter estimation, biological process model.

1 Introduction

The electroencephalogram (EEG) is a representative signal informing about the state of the brain [1]. The shape of the wave may contain useful information about brain pathology. EEG records during some epileptic seizures, Alzheimer's, and Parkinson's disease are much more ordered oscillatory than in healthy records [1-4]. The bigger problem is distinguishing subtle changes in brain wave patterns as the seizure spreads. Some changes are very subtle highly subjective, the symptoms may appear at random in the time scale. Therefore, the EEG signal parameters, extracted, analyzed, and modeled using computers, are highly useful in diagnostics. The analysis of EEG relies mainly on time-frequency analysis [5-9], wavelet analysis [8,10-11]. In the case of newborns due to strong non-stationary properties of EEG signals, Nabeel and Sadiq [12] proposed Adaptive Directional Time-Frequency Distribution (ADTFD) can lead to better classification of ictal EEG signals. The ADTFD gives a highly concentrated time-frequency representation of spikes and sinusoids. In turn, in many hardware

ICCS Camera Ready Version 2022
To cite this paper please use the final published version:
DOI: 10.1007/978-3-031-08757-8_18

implementations of automatic epilepsy detection, wavelet transforms, principal component analysis, Hilbert-Huang transform, and support vector machines [13-14]. Several types of entropy, i.e. sample, multiscale, and permutation entropy are used in the analysis of seizure spread. The experimental results obtained for 2 seconds EEG sequences show that the mean value of permutation entropy gradually decreases from the seizure-free (pre- and post-ictal) to the seizure phase [13]. Equally important parameters that measure the complexity of signal are Hjorth's parameters: activity, mobility, and complexity, which are useful for the quantitative description of the EEG. EEG modeling is also based on its non-stationary nature and includes i.e. random and back-propagation (BP) neural networks and coupled oscillators [15-21]. The system described in [16] determines the areas with the highest activity of spikes/poly-spikes of the signal received for one channel. In addition to the automatic selection, these discharges are also possible to verify and possibly change manually.
In the article, we have presented a modified variant of the deterministic duffing Van der Pol oscillator model, proposed in previous works by Ghorbanian et all, to model healthy and Alzheimer's disease signals [2-3]. In our earlier works, we have used this model to analyze epileptic ictal signals for the first time [20-21]. The current study is a continuation of this research.

An important goal of the article is to determine the relationship between the parameters, model sizes, and patterns of seizure waves. The study is an attempt to learn and understand the mechanisms accompanying the following five epileptic conditions: the onset of seizures, sequences with leg movement, records during automatic movements, related to the state of confusion, and final state of the seizure, registered in one patient. Another purpose of the paper is to evaluate the possibilities of differentiating epileptic states as above based on the parameters of the duffing Van der Pol oscillator model determined for the real EEG signal. We are driven by the motivation to use the obtained results in an expert system to support the process of medical diagnostics.

Similar to the articles [2-3], the possibility of extracting frequency bands for which the dominant values of the power spectra of real and generated are examined. Application of the deterministic duffing Van der Pol oscillator model to differentiate the same five phases of seizures was described in [21], however, without a statistical analysis of the optimal parameter values. In turn, the statistical analysis of the optimal values of the model parameters for the differentiation of only three groups of signals: pre-, ictal, and post-ictal, was carried out by us in [20]. The values of sample entropy of real EEG signals registered during five ictal phases were presented in [21], without comparison with the values of sample entropy obtained for the modeled signals. To our knowledge, so far in the literature, spectrograms have not been used to analyze signals from such precisely separated seizure phases: the onset, the confusion, and automatic movements.

The main achievement of the article is the confirmation that the statistical analysis of optimal values of three pairs of parameters of the duffing Van der Pol oscillator model: linear stiffness coefficient ς, nonlinear stiffness coefficient ρ, Van der Pol damping coefficient ε enable the differentiation of the individual phases of the seizure in short period seizure waves, e.g. fast and slow waves. In addition, it has been shown that the power spectra of the real and generated signal are dominated by certain components in the frequency bands δ, θ, and α in each considered ictal stage.

ICCS Camera Ready Version 2022
To cite this paper please use the final published version:
DOI: 10.1007/978-3-031-08757-8_18

The article analyzes the distribution of the duffing Van der Pol oscillator parameters for five seizure states: the onset of seizures, sequences with leg movement, records during automatic movements, related to the state of confusion, and final state of the seizure, derived from 15 registered EEG sequences. The determined distributions are presented in the form of box plots, independently for each of the 6 parameters of the duffing Van der Pol model: linear stiffness coefficients ς_1 and ς_2, nonlinear stiffness coefficients ρ_1 and ρ_2, Van der Pol damping coefficients ε_1 and ε_2. We made a comparative time-frequency analysis of epileptic real signals and the corresponding signals generated by the duffing Van der Pol oscillator model. The analysis of average values of power spectra is performed for three real and three generated signals in given frequency ranges in each considered phase of the seizure and the relative error between the average power values of the real and generated signal spectrum in three determined frequency bands: σ, θ, and α are calculated. The sample entropy values of real and generated signals obtained for the onset, the tangled stage, and automatic movements are compared. The achieved results are verified based on spectrograms made for real signals.

2 Materials and Methods

2.1 EEG signals

EEG signals presented in this paper were recorded from a right-handed 55 aged female who takes Phenytoin, at Temple University Hospital and is seizure-free for 7 months [22]. A more detailed description of the patient and the test conditions can be found in [21]. We considered sequences 10 s (number of samples N=2500) registered by electrode T3: 3 sequences corresponding to the onset of the seizure, 3 sequences of the phase with leg movements, sequences with registered automatic movements, 3 sequences of the entanglement, and 3 sequences associated with the end of the seizure.

2.2 Duffing Van der Pol Oscillator

We based on the oscillator model described in the literature for the first time by Ghorbanian et all. The deterministic coupled system of duffing Van der Pol oscillators can be written as [2-3]:

$$\begin{aligned}
\dot{x}_1 &= x_3 \\
\dot{x}_2 &= x_4 \\
\dot{x}_3 &= -(\varsigma_1+\varsigma_2)x_1 + \varsigma_2 x_2 - \varsigma_1 (x_1)^3 - \rho_2 (x_1 - x_2)^3 + \varepsilon_1 x_3 (1 - x_1) \\
\dot{x}_4 &= \varsigma_2 x_1 - \varsigma_2 (x_1 - x_2)^3 + \varepsilon_2 x_4 \left(1 - (x_2)^2\right)
\end{aligned} \tag{1}$$

where ς is the linear stiffness coefficient, ρ is the nonlinear stiffness coefficient, associated with the strength of the duffing nonlinearity resulting in multiple resonant frequencies, ε is the Van der Pol damping coefficient related to the strength of Van der Pol

ICCS Camera Ready Version 2022
To cite this paper please use the final published version:
DOI: 10.1007/978-3-031-08757-8_18

nonlinearity. Parameters ς_1, ρ_1, ε_1 and ς_2, ρ_2, ε_2 belong to the first and second oscillator, respectively.

The velocity of the second oscillator is selected as the model output. The initial conditions are equal to: $x_1(0)=0$, $x_2(0)=1$, $x_3(0)=0$, $x_4(0)=0$. Eq. (1) is solved by Runge-Kutta iterative method.

2.3 Optimization scheme

Figure 1 presents a block diagram of the optimization scheme proposed in the paper. The optimization process is repeated for each signal of mentioned earlier set of 15 recorded EEG signals. To determine the number of the sequence we introduced the parameter d, where d=1,2,..,.15.

Before calculating the discrete Fourier transform of each sample of real and generates EEG sequence has been multiplied by the appropriate Blackman's window coefficient [2]. The discrete Fourier transform (DFT) can be rewritten as:

$$X^d(k)=\sum_{n=0}^{N-1} x_w^d(n)\,\omega_N(n,k) \tag{2}$$

where:

$\omega_N=\exp(-j2\pi nk/N)$ is the N^{th} root of unity.

According to Figure 1, the amplitude of DFT of the signal is normalized in the range of [0, 1]:

$$\hat{X}_d(k)=\frac{|X_d(k)|}{\max|X_d(k)|} \tag{3}$$

Next, the power of normalized DFT amplitude sequences in five major frequency bands are calculated according to the formula:

$$\hat{P}_d^v=\frac{1}{|S_v|}\sum_{k\in Sv}\left(\hat{X}_d(k)\right)^2 \tag{4}$$

where: v=1,…,5 is the number of the frequency band, Sv - set of discrete frequencies, corresponding to five major frequency bands [2]. The indexes v and Sv are presented in Table 1.

Table 1. The major EEG frequency bands.

Number of frequency band v	EEG band	Hz	S_v of discrete frequencies (k)
1	δ	1-4	{1,…,15}
2	θ	4-8	{16,…,31}
3	α	8-13	{32,…,51}
4	β	13-30	{52,…,119}
5	γ	30-60	{120,…,239}

ICCS Camera Ready Version 2022
To cite this paper please use the final published version:
DOI: 10.1007/978-3-031-08757-8_18

The power of normalized DFT amplitude of the generated signal is calculated in the same manner in the same way as shown in formula (4). Having the power averaged power for each frequency band of the real and generated signal with the determined values, we can determine the objective function L (5):

$$L(\Omega,\ d) = \sum_{v=1}^{5}\left(\hat{P}_d^v - \breve{P}^v\left(\varsigma_1,\varsigma_2,\rho_1,\rho_2,\varepsilon_1,\varepsilon_2\right)\right)^2$$
$$\Omega = \left[\varsigma_1,\varsigma_2,\rho_1,\rho_2,\varepsilon_1,\varepsilon_2\right] \tag{5}$$

where: L is the cost function, $\mathbf{\Omega}$ is the vector of design model variables, $0 \le \varsigma_{1,2} \le 200$, $0 \le \rho_{1,2} \le 100$, $0 \le \varepsilon_{1,2}$ are the decision variables of the optimization.

The optimization goal is error minimization:

$$\min_{\mathbf{\Omega}} L(\mathbf{\Omega},\ d)$$

The optimization has been carried out using a genetic algorithm (GA) in a Matlab environment with bult-in function ga. The optimization scheme is repeated for each pair of real sequences and the corresponding generated sequence.

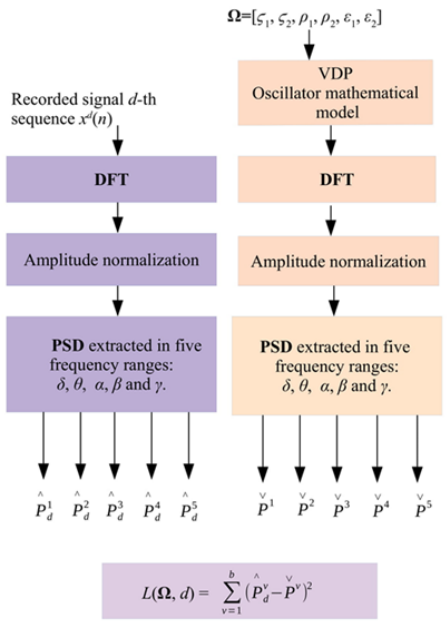

Fig. 1. Diagram of the optimization model.

3 Results

The analysis based on the optimal values of parameters, average values of the power spectrum of real and generated signals, the maximal difference between the power spectrum of generated and real signal, and the sample entropy of them is performed taking into account types of sequences. The estimated values of parameters are presented in

ICCS Camera Ready Version 2022
To cite this paper please use the final published version:
DOI: 10.1007/978-3-031-08757-8_18

the form of box plots, where the plots are made separately for each parameter of the model. Figure 2 shows the results obtained for the linear stiffness coefficient produces by the first oscillator. On the *x*-axis graph, separate states of seizures are marked as sequence no: 1 indicates the onset of seizures, 2 - sequences with leg movement, 3 - automatic movements, 4 is related to the state of confusion, and 5 determines the final state of the seizure. Low and comparable values of the parameter are obtained for the phases in which there are no changes in behavior, i.e. the onset of the seizure (marked as 1 in the graph and the end of the seizure marked as 5). High values of the parameter and large dispersion of the results, which reflect the height of the box, are achieved for the moments when there are large changes in the patient's behavior: leg movement and confusion.

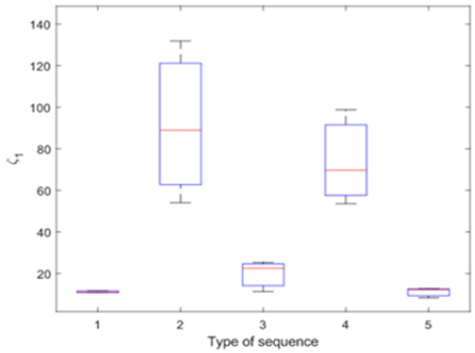

Fig. 2. The box chart of optimal values of the model's linear stiffness parameter ς_1.

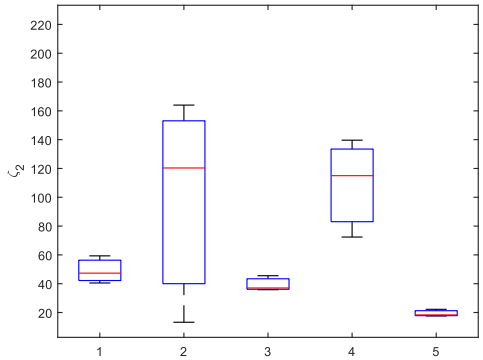

Fig. 3. The box chart of optimal values of the model's linear stiffness parameter ς_2.

Figure 3 has been created for the linear stiffness parameter generated by the second oscillator. Similar to the first diagram, we can distinguish two analogous phases with

ICCS Camera Ready Version 2022
To cite this paper please use the final published version:
DOI: 10.1007/978-3-031-08757-8_18

significantly greater dispersion of parameter values. Additionally, comparable median values optimal parameter values (marked with a red line inside the box) are obtained for the initial phase and with the accompanying automatic movements occurring in the patient. The low median value of the parameter also makes it possible to distinguish the final phase of the seizure. Low and comparable values of the parameter are obtained for the phases in which there are no changes in behavior, i.e. the onset of the seizure (marked as 1 in the graph and the end of the seizure marked as 5). High values of the parameter and large dispersion of the results, which reflect the height of the box, are achieved for the moments when there are large changes in the patient's behavior: leg movement and confusion.

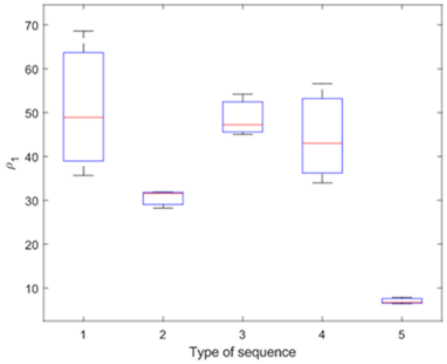

Fig. 4. The box chart of optimal values of the model's non-linear stiffness parameter ρ_1.

Figures 4-5 refer to the nonlinear stiffness coefficients, ρ_1 and ρ_2, respectively. In the initial phase of the seizure, high values of the non-linear stiffness parameter generated by the first oscillator are achieved. A negative correlation is also obtained for the state in which the patient moves her leg, i.e. low values of nonlinear parameters.

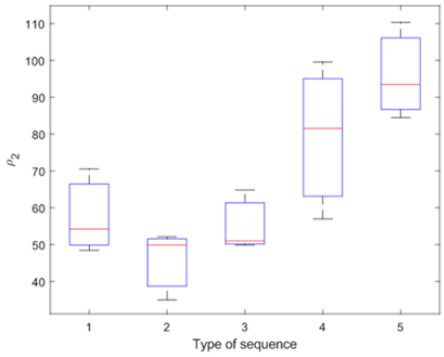

Fig. 5. The box chart of optimal values of the model's non-linear stiffness parameter ρ_2.

ICCS Camera Ready Version 2022
To cite this paper please use the final published version:
DOI: 10.1007/978-3-031-08757-8_18

The final stage of the seizure is characterized only by a high parameter value of ρ_2. Figures 6-7 present results achieved for the Van der Pol damping coefficients. For states marked as 1 and 3, the median of ε_1 values hovers around 5 and is different from the other two phases (4 and 5). Based on Figure 7, median, first and third quartile values of ε_2 are comparable in all phases.

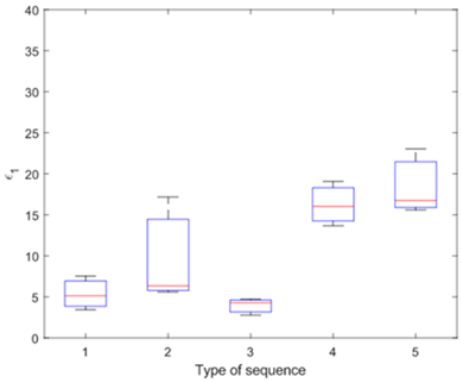

Fig. 6. The box chart of optimal values of the model's Van der Pol damping parameter ε_1.

In a further step power spectra of real signals (marked in blue) and generated by the oscillator model (red dotted line) are compared. Figure 8 shows the power spectra of real and generated EEG signals recorded during the entanglement state. Differences in the values of the power spectrum of the real and generated signal are obtained for α and β frequencies. From about 30 Hz, a rightward shift in the spectrum of the generated signal is observed.

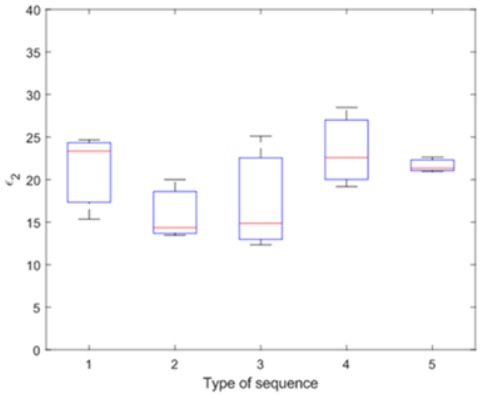

Fig. 7. The box chart of optimal values of the model's Van der Pol damping parameter ε_2.

ICCS Camera Ready Version 2022
To cite this paper please use the final published version:
DOI: 10.1007/978-3-031-08757-8_18

Table 2 shows the average values of power spectra of three real and three generated signals in given frequency ranges in each considered phase of the seizure, where R denotes recorded data and G refers to generated signal. According to Figure 8, the results obtained in Table 2 show that the power spectra of the real and generated signal are dominated by components in the frequency bands: δ, θ, and α (high average values of the power spectrum in these bands for each considered phase from Table 2).

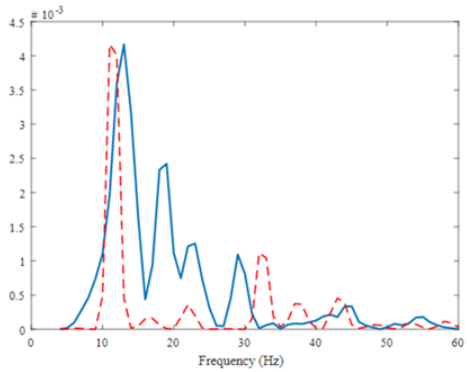

Fig. 8. Comparison of the power spectrum of the real and the generated signal corresponding to the entangled state.

Table 3 presents the average relative error between the average power values of the real and generated signal spectrum in the three dominant frequency bands of spectrograms: δ, θ, and α obtained in each determined phase of seizures. It can be seen clearly, that the stage of the seizure of low values of the determined ratio is the final state for each described EEG band. Interestingly, high values of average percentage power error for δ (equal to 50%) and low (5.6%) for θ are achieved for the seizure phases related to the patient's movements (marked in Table as 2 and 3). The α band is characterized by high power error values of the real and generated signal spectrum in the phases (1-4) close to 30% without the end of the seizure.

Table 2. The average power spectrum values of the real and generated signal in all discussed phases of seizure.

Phase		EEG band				
		δ	θ	α	β	γ
1 onset	R	0.1860	0.2300	0.1200	0.0180	0.0010
	G	0.1970	0.2100	0.0900	0.0060	0.0006
2 leg	R	0.0015	0.0038	0.0016	0.0004	0.0004
movement	G	0.0017	0.0039	0.0014	0.0005	0.0003
3 automatic	R	0.0006	0.0024	0.0008	0.0003	0.0006
movements	G	0.0008	0.0028	0.0010	0.0004	0.0001
4 confusion	R	0.0006	0.0046	0.0007	0.0005	0.0003
	G	0.0005	0.0050	0.0004	0.0002	0.0002
5 final	R	0.1867	0.2150	0.1301	0.0067	0.0005
seizure state	G	0.1837	0.2167	0.1300	0.0080	0.0001

ICCS Camera Ready Version 2022
To cite this paper please use the final published version:
DOI: 10.1007/978-3-031-08757-8_18

Table 3. The average percentage power error values of the real and generated signal spectrum in three determined frequency bands: δ, θ, and α.

Phase	EEG band		
	δ	θ	α
1 onset	7.9%	16.7%	30.0%
2 leg movement	50.0%	5.6%	30.0%
3 automatic movements	50.0%	5.6%	30.0%
4 confusion	24.5%	22.0%	36.9%
5 final seizure state	7.0%	10.9%	14.0%

To examine the nature of the EEG signal more closely, spectrograms are made for a rectangular window of 512 sequence samples. The y axis of the spectrogram shows frequency and the x axis-time.

Figure 9 is made for sequences when the first panic pattern was registered. The spectrogram is dominated by low frequencies corresponding to waves δ, θ, and α. In the ranges of time 0-2 and 19-20 s of the seizure, spectrum building high frequencies (γ) is observed. In the time interval between 5 and 13 s the spectrum stabilizes to δ, θ, α, and β frequencies. From 14 to 18 s the components associated with complex slow waves dominate in the spectrum (rhythms δ, θ) and fast amplitude peak waves of low amplitude (α rhythm), which may be due to the patient's hyperventilation.

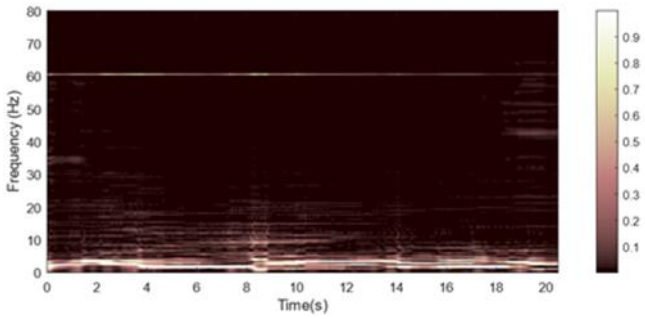

Fig. 9. A spectrogram of real EEG signal presented the onset of the seizure (marked in Tables 2-3 as phase 1).

Figures 10 and 11 present spectrograms obtained for the real signals during the confusion and automatic movements. The spectrogram presented in Figure 10 shows a stable spectrum of all considered frequency bands. In the case of automatic movements, three phases can be distinguished in the spectrogram: in the 0-5 s time interval, δ, θ, and α frequencies dominate, between 6 and 10 s, also higher β and γ bands are present, from 10 to 20 seconds in the spectroscope there are frequencies up to 30 Hz. Next, a comparison of the calculated entropy value for real and generated signals for three phases in Figures 9-11 is analysed. The results are summarized in Table 4.

ICCS Camera Ready Version 2022
To cite this paper please use the final published version:
DOI: 10.1007/978-3-031-08757-8_18

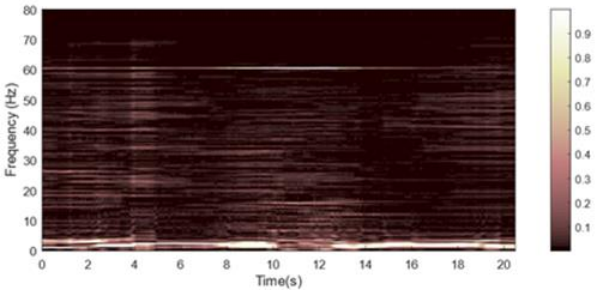

Fig. 10. A spectrogram of real sequences for entangled stage (marked in Tables 2-3 as phase 4).

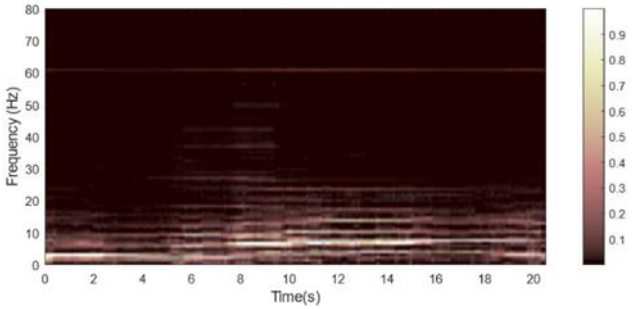

Fig. 11. A spectrogram of real sequences achieved during automatic movements (presented in Tables 2-3 as phase 3).

Table 4. The sample entropy of real and corresponding generated signals presented in figures 9-11.

Phase	Sample entropy	
	R	*G*
1	0.24	0.07
3	0.08	0.05
4	0.12	0.06

4 Discussion and conclusion

Based on Table 2, it can see clearly that the dominant frequency bands in the power spectrum of signals presenting the complex temporal seizure are δ, θ, and α in all considered phases of the seizure. The plot obtained with the classical FFT analysis of the real signal is comparable with the plot obtained for the generated signal (see Figure 8). In β and γ frequency ranges, the differences between the real signals and the corresponding generated signals occur in the average value of the spectra, i.e. average power spectrum in the onset obtained for real signal in β range is equal to 0.018 vs. 0.0006 for

ICCS Camera Ready Version 2022
To cite this paper please use the final published version:
DOI: 10.1007/978-3-031-08757-8_18

generated signal, and for the entanglement 0.0005 vs. 0.0002, respectively (Table 2). The results from Table 3 show that in states where the patient's anxious behavior affects the recording of brain waves (i.e. movements, the entanglement), high values of the coefficient are obtained, calculated as the average relative power error of generated and real signal in two determined frequency bands: σ and α, and low values-for θ band. The ratio values from Table 3 allow to distinguish sequences related to movements (marked as 2 and 3), in which similar average percentage power error values are obtained. Based on the low value of the error coefficients obtained for the δ band, the initial and final stages of the seizure (marked as 1 and 5) can be also eminent from those in which the propagation of the seizure waves took place over time. The proposed deterministic model encounters difficulties with chaotic, difficult to interpret waveforms related to the patient's behavior. An experienced clinician also had a problem with interpreting these states, who considered the record of the signal related to the movement of the leg difficult to assess. Based on the box plots, high dispersions can be seen in the optimal values of the linear stiffness parameters for the phases in which the patient is aroused (the second and fourth boxes in Figures 2-3). On the other hand, for the states occurring without changing the behavior of the patient (the first and fifth box in Figures 4-5), there is a slight variation in the values of the parameters. Considering the nonlinear parameters of stiffness, we note an inverse relationship, greater differentiation in the parameter values for the initial state (first box), and smaller for the leg movement (third box) on Figs. 4-5. The appearance of dispersion in the optimal values of the parameters of signals generated in the same phase of the seizure indicates the occurrence of intra-individual variability. Intra-individual variability significantly influences the recording of real EEG signals. This indicates that the proposed model, in this respect, maintains the physiological dependencies occurring in real signals.

Despite the presence of dispersion in the optimal values of the model parameters, their median, maximum or minimum values, as discussed in section 3, allow determining the seizure phases and wave patterns associated with these states.

Low optimal values of linear and nonlinear stiffness parameters are noted in the case of recording low waves, the terminal phase of the seizure. Small optimal values of linear parameters and higher nonlinear parameters accompany the occurrence of wave waves with a complex of slow waves (the onset and low optimal values of linear parameters and higher nonlinear parameters accompany the occurrence of wave waves with a complex of slow waves). High values of linear and nonlinear parameters generate fast waves of high amplitude (hand movement, entanglement).

Besides it allows us to determine the parameters of the oscillator model, with the help of which we could differentiate the individual phases of the seizure in a short period, and thus differentiate seizure waves, e.g. fast and slow waves. In depth study of generated signals, including time-frequency analysis, is to add a stochastic component to the model.

ICCS Camera Ready Version 2022
To cite this paper please use the final published version:
DOI: 10.1007/978-3-031-08757-8_18

References

1. Acharya, U.R., Molinari, F., Vinitha, S., Chattopadhyay S.: Automated diagnosis of epileptic EEG using entropies. Biomedical Signal Processing and Control, 4(7), 401-408 (2012).
2. Ghorbanian, P.: Non-Stationary Time Series Analysis and Stochastic Modeling of EEG and its Application to Alzheimer's Disease. [Doctoral dissertation, Villanova University] (2014).
3. Ghorbanian, P., Ramakrishnan, S., Ashrafiuon, H.: Stochastic non-linear oscillator models of EEG: the Alzheimer's disease case. Frontiers in Computational Neuroscience, 9(48) DOI: 10.3389/fncom.2015.00048. (2015).
4. Botcharova, M.: Modelling and analysis of amplitude, phase and synchrony in human brain activity patterns. [Doctoral dissertation, University College London] (2014).
5. Yuan Y., Xun G., Jia K., Zhang A.: A multi-view deep learning method for epileptic seizure detection using short-time fourier transform. ACM-BCB '17: Proceedings of the 8th ACM International Conference on Bioinformatics, Computational Biology,and Health Informat-icsAugust, pp.213–222. https://doi.org/10.1145/3107411.3107419. (2017).
6. Szuflitowska B., Orlowski P.: Comparison of the EEG signal classifiers LDA, NBC and GNBC based on time-frequency features. Pomiary Automatyka Robotyka, 2 (21), 39-45 (2017).
7. Li M,. Chen W.: FFT-based deep feature learning method for EEG classification. Biomedical Signal Processing and Control, vol. 66, 102492, (2021).
8. Chen G., XieT.D., Bui, Krzyżak A.: Automatic Epileptic Seizure Detection in EEG Using Nonsubsampled Wavelet–Fourier Features. Journal of Medical and Biological Engineering, vol.37, 123–131(2017).
9. Khan N.A., Ali S.: Classification of EEG Signals Using Adaptive Time-Frequency Distributions. Metrology and Measurement Systems, 23(2), 251-260 (2016).
10. Kocadaglia O., Langarib R.: Classification of EEG signals for epileptic seizures using hybrid artificial neural networks based wavelet transforms and fuzzy relations. Expert Systems with Applications, vol. 88, 419-434 (2017).
11. Alturki F.A., AlSharabi K., Abdurraqeeb A.M., Aljalal M.: EEG Signal Analysis for Diagnosing Neurological Disorders Using Discrete Wavelet Transform and Intelligent Techniques. Sensors, 21(20), 6932; https://doi.org/10.3390/s21206932 (2021).
12. Zhang Q., Hu Y., Potter T., Li R., Quach M., Zhang Y.: Establishing functional brain networks using a nonlinear partial directed coherence method to predict epileptic seizures. Journal of Neuroscience Methods, vol. 329, 108447 (2020).
13. Revati S. V., Baskar V., Martin B.M., Sundhararajan N.D.: Energy Distribution and Coherence-Based Changes in Normal and Epileptic Electroencephalogram. Smart Intelligent Computing and Applications, 625-635 (2019).
14. Albera I. et all: ICA-based EEG denoising: a comparative analysis of fifteen methods. Bulletin of the Polish Academy of Sciences: Technical Sciences, 60 (3), http://doi.org/10.2478/v10175-012-0052-3 (2012).
15. Rafiammal S.S., Najumnissa D., Anuradha G., at all: A Low Power and High Performance Hardware Design for Automatic Epilepsy Seizure Detection. Int Journal of Electronics and Telecommunications, 65(4), 707-712 (2019).

ICCS Camera Ready Version 2022
To cite this paper please use the final published version:
DOI: 10.1007/978-3-031-08757-8_18

16. Gaidar V., Sudakov O.: Design of Wearable EEG Device for Seizures Early Detection. Int Journal of Electronics and Telecommunications, 67(2), 187-192 . (2021).
17. Liu, L.: Recognition and Analysis of Motor Imagery EEG Signal Based on Improved BP Neural Network. IEEE Access, 7, 47794 – 47803 (2019).
18. Gandhi, T., Bhowmik P., Mohapatra, A., Das, S., .at all: Epilepsy Diagnosis Using Combined Duffing Oscillator and PNN Model. Journal of Bioinformatics and Intelligent Control, 1(1), 64-70 (2012).
19. Tabi, C., B.: Dynamical analysis of the FitzHugh-Nagumo oscillatons through a modified Van der Pol equation with fractional-order derivative term. International Journal of Non-Linear Mechanics, 105, 173-178 (2018).
20. Szuflitowska, B., Orlowski, P.: Statistical and physiologically analysis of using a Duffing-van der Pol oscillator to modeled ictal signals. 16th Int. Conf. on Control, Automation, Robotics and Vision (ICARCV), pp.1137-1142. DOI. ieee.org/document/9305339 (2020).
21. Szuflitowska B., Orlowski P.: Analysis of Complex Partial Seizure Using Nonlinear Duffing Van der Pol Oscillator Model. In: Paszynski M., Kranzlmüller D., Krzhizhanovskaya V.V., Dongarra J.J., Sloot P.M. (eds) Computational Science – ICCS 2021. ICCS 2021. Lecture Notes in Computer Science, vol 12745. Springer, Cham. https://doi.org/10.1007/978-3-030-77970-2_33 (2021).
22. Obeid, I., Picone, J., Harabagiu, S.: Automatic Discovery and Processing of EEG Cohorts from Clinical Records. In Big Data to Knowledge All Hands Grantee Meeting (p. 1). Bethesda, Maryland, USA: National Institutes of Health. [Online]. https://pubmed.ncbi.nlm.nih.gov/24509598/ (2016).

ICCS Camera Ready Version 2022
To cite this paper please use the final published version:
DOI: 10.1007/978-3-031-08757-8_18